Taylor & Francis
Taylor & Francis Group

RESEARCH ARTICLE

🔓 OPEN ACCESS ⓜ Check for updates

A comparative study on the *in vitro* and *in vivo* antitumor efficacy of icaritin and hydrous icaritin nanorods

Haowen Li[a], Yijing Li[a], Hui Ao[a], Jingxin Fu[a], Yifei Guo[a], Meihua Han[a], Xueying Yan[b], Xi Chen[a] and Xiangtao Wang[a]

[a]Institute of Medicinal Plant Development, Chinese Academy of Medical Sciences & Peking Union Medical College, Beijing, PR China; [b]College of Pharmacy, Heilongjiang University of Chinese Medicine, Harbin, PR China

ABSTRACT

Icaritin (ICT) and hydrous icaritin (HICT) are two similar flavonoids compounds isolated from *Epimedium* Genus. This is the first comparative study on their *in vitro* and *in vivo* antitumor effects. Nanorods (NRs) were prepared for ICT and HICT by anti-solvent precipitation method using D-alpha tocopherol acid polyethylene glycol succinate (TPGS) as a stabilizer. The prepared ICT-NRs and HICT-NRs had similar diameter (155.5 nm and 201.7 nm), high drug loading content ($43.30 \pm 0.22\%$ and $41.08 \pm 0.19\%$), excellent stability and a similar sustaining drug release manner. Nanorods improved the *in vitro* toxicity against 4 different cancer cells in contrast to free ICT or free HICT; however, no significant difference was observed in this regard between ICT-NRs and HICT NRs. In the *in vivo* study on the anticancer efficacy on MCF-7 and PLC/PRE/5 tumor-bearing mice model, HICR-NRs displayed certain advantage over ICT NRs with higher tumor inhibition rate.

Introduction

Icaritin (ICT), also named anhydroicaritin in some paper (Zheng et al., 2017), is one of the major bioactive flavonoid compounds isolated from traditional Chinese medicine *Epimedium* Genus (Li et al., 2012; Zhao et al., 2015; Hu et al., 2016; Liao et al., 2016; Zhang, 2016; Wang et al., 2017) and is selected as the chemical index for quality control of Herba Epimedii in Chinese Pharmacopeia (Commission, 2010; Li et al., 2015). ICT exhibits an extensive range of biological and pharmacological activities, such as neuroprotection (Wang et al., 2009), cardiac protection (Zhu & Lou, 2005; Wo et al., 2008; Wang et al., 2009; Zhang et al., 2015), anti-inflammation, immunomodulation (Li et al., 2012; Lai et al., 2013; Liao et al., 2016), and multidrug resistance reversal activity (Liu et al., 2009). Increasing studies proved ICT could suppress growth of different kinds of cancers including breast cancer (Wang & Lou, 2004; Guo et al., 2011; Tiong et al., 2012), prostate cancer (Huang et al., 2007; Sun et al., 2015; Hu et al., 2016; Sun et al., 2016), bladder cancer (Pan et al., 2016), endometrial cancer (Tong et al., 2011), glioblastoma (Han et al., 2015; Li et al., 2016), colorectal cancer (Li et al., 2016 Zhou et al., 2016; Zhou et al., 2017), lymphoma (Li et al., 2014; Wu et al., 2015), hepatocellular carcinoma (He et al., 2010; Sun et al., 2013; Zhao et al., 2015; Zhang et al., 2016; Lu et al., 2017), lung cancer (Zheng et al., 2014; Wang et al., 2015), osteosarcoma (Wang & Wang, 2014), chronic/acute

myeloid leukemia (Zhu et al., 2011; Li et al., 2013), esophageal cancer(Han et al., 2018) and hematological malignancies (Li et al., 2013; Zhu et al., 2015). Ye and Lou's researches have proved that ICT could induce the proliferation of estrogen receptor (ER)-positive breast cancer MCF-7 cells at sub-micromolar levels. What's more, ICT could provoke apoptosis of both ER-positive MCF-7 cells and ER-negative MDA-MB-453 breast cancer cells at micromolar level (Wang & Lou, 2004; Ye & Lou, 2005; Guo et al., 2011; Tiong et al., 2012; Hu et al., 2016). Based on its excellent therapeutic effect on different human malignancies, ICT has been participated into several clinical trials including hepatocellular cancer (phase III, ClinicalTrials.gov Identifier: NCT03236636), PD-L1 positive advanced hepatocellular cancer (phase III, ClinicalTrials.gov Identifier: NCT03236649) and advanced breast carcinoma (phase I, ClinicalTrials.gov Identifier: NCT01278810) (Hao et al., 2019).

Hydrous icaritin (HICT), is also a bioactive flavonoid compound derived from *Epimedium* Genus. It is chemically close to ICT, with the only difference of the chemical group at C-8, being the isopentane group for ICT while the −2′-hydroxyl-isopentyl group for HICT (Figure 1(a,b)). Comparatively, limited investigation has been performed on the biological activity of HICT. It was reported that peritumorally injected HICT/DMSO solution significantly inhibited renal tumor growth at a dose of 10 mg/kg (Li et al., 2013). Intraperitoneal
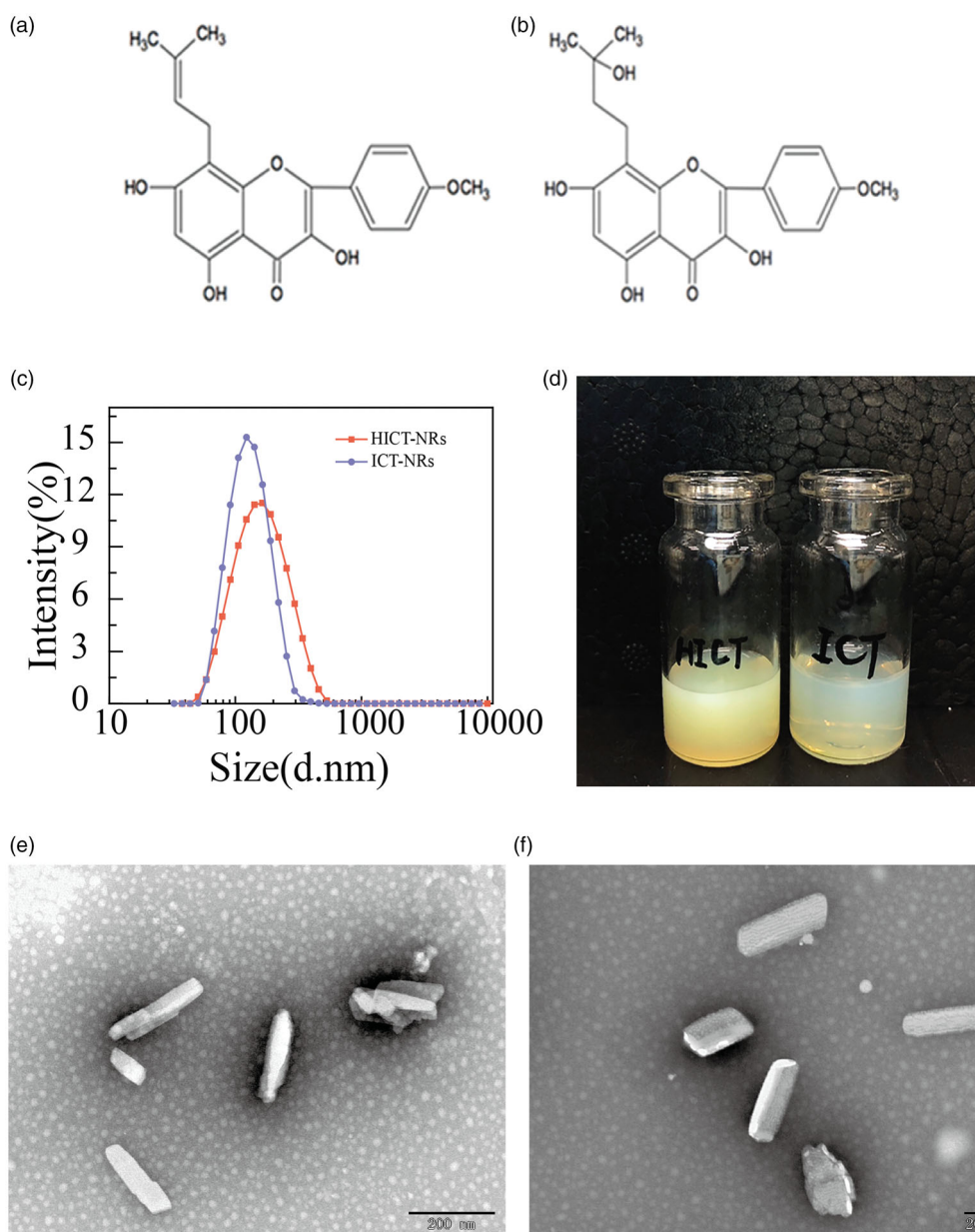

Figure 1. Chemical structure of ICT and HICT and characterization of ICT/HICT-NRs. (a) Chemical structure of anhydrous ICT. (b) Chemical structure of HIICT. (c) The particle size of HICT-NRs (left) and ICT-NRs (right) measured by DLS. (d) Photograph of ICT-NRs and HICT-NRs. (e) TEM image of ICT-NRs. (f) TEM image of HICT-NRs.

injected HICT solution (30 mg/kg, 5 times a week) could effectively delay the progression of prostate cancer and significantly increase the survival of TRAMP mice (Hu et al., 2016). Our preliminary research demonstrated HICT showed similar *in vitro* antitumor activity to that of ICT against several cancer cell lines, and we recently found HICT nanorods displayed a high tumor inhibition rate of 70.4% against MCF-7 breast cancer *in vivo*(Wang et al., 2020). HICT had estrogen-like effect and hepatoprotective effect (Liu et al., 2014).

Since ICT has shown very good antitumor efficacy and is now in the phase III clinic trial. HICT, with quite similar chemical structure and *in vitro* cytotoxicity against tumor cells, deserves attention and systemic investigation. Thus, in this paper, a comparative study on HICT and ICT was performed to investigate the potential application of HICT in antitumor treatment. Like most flavonoids, both ICT and HICT exhibit poor water solubility and widespread first-pass metabolism,

resulting in poor oral bioavailability (Yan et al., 2008; Zhang & Zhang, 2017). So, rod-like nanosuspensions (nanorods) were prepared for both ICT and HICT to compare their *in vitro* properties and *in vivo* anti-tumor efficacy on hepatic cancer and breast cancer mice models.

Materials and methods

Materials

ICT was purchased from Chengdu Ruifensi biotechnology Co. Ltd. (Chengdu, China). HICT was purchased from Nanjing DASF biotechnology Co. Ltd. (Nanjing, China). 1,2-distearoyl-sn-glycero-3-phosphoethanolamine-N- [methoxy (polyethylene glycol)-2000) (DSPE-mPEG2000) was from Shanghai ToYong biotechnology Co. Ltd. (Shanghai, China). Pluronic F-68 (F-68), Pluronic F-127 (F-127) and 3-(4, 5-dimethylthiazol-2-yl)-2, 5-diphenyltetrazolium bromide

(MTT) were supplied by Sigma Aldrich (St Louis, MO). D-alpha tocopherol acid polyethylene glycol succinate (TPGS) was purchased from Xi'an Healthful Biotechnology Co. Ltd. (Xi'an, China). Methoxy (polyethylene glycol)2000–poly (ε-caprolactone)2000 (mPEG2000–PCL2000) was bought from Jinan Daigang Biomaterial Co. Ltd. (Jinan, China). Paclitaxel (PTX) injection was provided by the Beijing union pharmaceutical factory (Beijing, China). Acetonitrile was High-performance liquid chromatography (HPLC) grade provided by Fisher Scientific (Pittsburgh, PA). All other reagents were analytical pure. Deionized water was used in the experiments.

Cell lines and animals

The MCF-7 (human breast carcinoma), 4T1 (murine mammary carcinoma), PLC/PRF/5 (human hepatic carcinoma), HepG2 (human hepatic carcinoma), and HUVEC (human umbilical vein endothelial cell) cell lines used in this research were supplied by Chinese Infrastructure of Cell Line Resource (Beijing, China). MCF-7 cells were cultured with Dulbecco's modified Eagle's medium (DMEM). 4T1 cells were cultivated with Roswell Park Memorial Institute 1640 medium (RPMI 1640). PLC/PRF/5 and HepG2 cells were cultured with Minimum Essential medium (MEM). HUVEC cells were cultured with Ham's F12 medium (F12). Different cells were cultured in specific media with 10% fetal bovine serum (FBS), penicillin (100 U/mL), and streptomycin (100 U/mL) at 37 °C with 5% CO_2 (Sanyo, Osaka, Japan). All the media used were purchased from HyClone. FBS, penicillin and streptomycin were purchased from Gibco.

Female NU/NU nude mice (6–8 weeks, 20 ± 2 g) were provided by Vital River Lab-oratory Animal Technology Co., Ltd. (Beijing, China). All mice were provided with a 70% humidity under 12 h light–dark cycle conditions at and 25 °C for 5 days before experiments. The animal experiments followed the guidelines for Ethical and Regulatory for Animal Experiments of The Institute of Medicinal Plant Development (IMPLAD, license no. SYXK 2018-0020), China.

Preparation of HICT or ICT nanorods

ICT nanorods (ICT-NRs) and HICT nanorods (HICT-NRs) were prepared using antisolvent precipitation method (Han et al., 2014). Specifically, ICT or HICT crystalline powder, together with stabilizer, was dissolved in 500 μL of dimethyl sulfoxide (DMSO) to get an organic solution, then the organic phase was slowly injected into the water at specific temperature under 250 W ultrasonication. Next, the suspensions were centrifuged at 13000 rpm for 20 min, and the sediment was dispersed uniformly with deionized water under ultrasonication at 250 W for 20 min, followed by homogenization at 25 °C for 10 cycles under 1500 bar to obtain ICT-NRs or HICT-NRs. mPEG2000-PCL2000, mPEG2000-DSPE were dissolved in DMSO together with ICT or HICT when used as stabilizers, while Pluronic F68, F127 and TPGS were dissolved in the deionized water under sonication.

Physicochemical characterizations of HICT and ICT nanorods

Particle size measurement

The mean particle size, polydispersity index (PDI), and zeta potential of ICT-NRs or HICT-NRs were measured using a dynamic light scattering (DLS, Zetasizer Nano ZS, Malvern Instruments, UK) at room temperature. Each sample was measured three times with 12 scans.

Morphology observation

The morphological characterization of ICT-NRs or HICT-NRs was observed using a JEM-1400 transmission electron microscope (JEOL, Tokyo, Japan). 5 μL of ICT or HICT nanorods was dropped on a 300-mesh copper grid, air-dried, then colored with 2% (w/v) uranyl acetate for observation under the microscope.

X-ray diffraction (XRD)

XRD patterns of samples (ICT or HICT-NRs lyophilized powder, ICT or HICT crystalline powder, TPGS, and ICT or HICT crystalline powder with TPGS physical mixture) were detected by an X-ray diffractometer (DX-2700, China) Cu-Kα radiation generator set at 100 mA and 40 kV. All samples were scanned over an angular range of 3–80°, with a step size of 0.02° and a count time of 3 s per step.

Differential scanning calorimetry (DSC)

DSC thermal profiles of all powder samples (ICT or HICT-NRs lyophilized powder, ICT or HICT crystalline powder, TPGS, and ICT or HICT crystalline powder with TPGS physical mixture) were detected by a differential scanning calorimeter (Q200, TA Instruments, New Castle, DE). 5 mg of each sample put and sealed in standard aluminum pans was measured from 0 °C to 500 °C with a scanning rate of 10 °C/min under nitrogen environment.

Drug loading content

Specific weight of lyophilized nanorods was dissolved in a certain amount of methanol to determine drug loading content (DLC) of ICT-NRs or HICT-NRs. The concentration of ICT or HICT was determined by HPLC. The DLC was calculated by equation (1)

$$DLC\ (\%)\ = V \cdot C/W\ \times\ 100 \tag{1}$$

where V is methanol volume, C is ICT or HICT concentration, and W is the weight of lyophilized ICT or HICT nanorods.

High-performance liquid chromatography (HPLC) analysis

The concentration of ICT or HICT was determined by an HPLC apparatus (DIONEX Ultimate 3000, Germering, Germany). A Symmetry C18 column (4.6 mm × 250 mm, 5 μm; Dr. Maisch GmbH, Germany) was used for chromatographic separation at 25 °C. The moving phase was composed of acetonitrile and 0.1% acetic acid (68:32, v/v). The flow rate was 0.6 mL/min. The UV detection wavelength was

270 nm (UV detector, DIONEX). The methods were subjected to validations by specificity, linearity, intra- and inter-precision and limit of quantification. The methods for both ICT and HICT provided good linearity ($R^2 \leq 0.999$) over a concentration range of 5–100 μg/mL with the intra- and inter-precision of less than 2.0% and 1.0%, respectively, and LOQ of 500 ng/mL.

Stability of nanorods in various physiological solutions

To study whether physiological solutions would influence the stability of ICT-NRs and HICT-NRs or cause aggregation, the in vitro stability investigation was performed. ICT or HICT nanorods were, respectively, well mixed with 10% glucose and 1.8% NaCl (1:1,v/v), or with PBS (pH 7.4), rat plasma, artificial gastric and intestinal fluid (1:4, v/v), followed by incubation at 37 °C. 1 mL of the incubated solution was taken out and measured for particle size change at different time intervals. Each experiment was conducted in triplicate.

Hemolysis assay

To investigate the safety of the obtained ICT or HICT nanorods for intravenous injection, hemolysis rates were tested using healthy rat red blood cells (RBCs). Fresh rat blood was centrifuged at 3500 rpm for 15 min to remove plasma, then RBCs were washed 3 times with normal saline (NS) and diluted to 4% (v/v) concentration finally. Different concentrations of ICT or HICT nanorods were adjusted to be isotonic and respectively mixed (1:1, v/v) with the RBCs suspensions (experimental groups). The RBC suspension was mixed (1:1, v/v) with deionized water (positive control) and NS (negative control), respectively. In addition, different concentrations of ICT or HICT nanorods were mixed (1:1, v/v) with deionized water (blank control). The mixtures were incubated at 37 °C for 4 h and then centrifuged at 3500 rpm for 5 min. The absorbance value of supernatant was detected at 540 nm with ELISA plate reader (Biotek, Winooski, VT, USA). Hemolysis rate was calculated as follows:

$$\begin{aligned} &\text{Hemolysis rate }(\%) \\ &= (A\text{ sample} - A\text{ negative} - A\text{ blank}) \qquad (2) \\ &/(A\text{ positive} - A\text{ negative}) \times 100 \end{aligned}$$

where A sample is experimental group's absorbance value, A negative is negative control group's absorbance value, A blank is blank control group's absorbance value, and A positive is positive control groups' absorbance value. Each sample was carried out in triplicate.

In vitro drug release behavior

In vitro behavior of drug release from ICT or HICT nanorods was performed as follows. PBS containing 0.5% (w/v) Tween 80 (pH 7.4) was chosen as dissolution medium. ICT or HICT nanorods (4 mL, 300 μg/mL) were sealed in dialysis tubes (molecular weight cut off (MWCO): 8000–14000, Sigma, USA). The dialysis tubes were immersed into 2 L of dissolution medium and incubated at 37 °C under continuous stirring (100 rpm). 200 μL of internal liquid was taken out from the

dialysis tubes at special time intervals, and the same volume of fresh release medium were supplied into the dialysis bags. The dissolution medium was renewed every 24 h. The cumulative release of ICT or HICT nanorods was calculated according to the reduction of ICT or HICT inside the dialysis tubes (Hong et al., 2016). The concentration of ICT or HICT was analyzed by HPLC. The above experiments were performed in triplicate.

In vitro cytotoxicity assay

In vitro cell cytotoxicity of ICT or HICT nanorods against MCF-7, 4T1, PLC/PRF/5, HepG2, and HUVEC cells were evaluated using MTT assay. Typically, 150 μL of cells (cell density: 10000 cells/mL) were cultured in 96-well plates overnight at 37 °C in 5% CO$_2$. Then different concentrations of ICT nanorods, HICT nanorods (diluted with culture medium), free ICT and free HICT (dissolved in DMSO, diluted with culture medium, DMSO final concentration $\leq$ 0.1%, equivalent to 0.015 M) were added to each well and incubated for 48 h. Then, the cells were dealt with 20 μL of MTT solution (5 mg/mL in PBS) for 4 h. Subsequently, the medium was decanted, 150 μL of DMSO was added to dissolve bottom formazan crystals. The optical density (OD) value was detected at a maximum absorbance of 570 nm using ELISA plate reader (Biotech, Winooski, VT, USA). The cell viability rate of was calculated by equation (3):

$$\text{Cell viability rate }(\%) = \text{ODe}/\text{ODc} \times 100 \qquad (3)$$

where ODe is OD value of experimental group and ODc is OD value of the control group.

The half-inhibitory concentration (IC50) value of each group was calculated by GraphPad Prism software, Version 7 (GraphPad Software, Inc., La Jolla, CA, USA).

In vivo antitumor activity on MCF-7 and PLC/PRF/5 tumor-bearing mice

In vivo antitumor efficacy of ICT or HICT nanorods was performed on two different mice models: MCF-7 tumor-bearing NU/NU mice and PLC/PRF/5 tumor-bearing NU/Nu mice. Female nude NU/NU mice were inoculated with 0.2 mL of MCF-7 cells (or PLC/PRF/5 cells) suspension (5.0×10^7 cells/mL) subcutaneously in the right armpit. The tumor-bearing mice were randomly divided into 7 groups (7 mice per group) when tumor volume reached around 100 mm^3. The mice were injected with NS (negative control group), paclitaxel injection (positive control group, 8 mg/kg), ICT-NRs (40 mg/kg), HICT-NRs (40 mg/kg) via tail vein every two days, or administered with ICT-NRs, HICT-NRs, free ICT suspensions and free HICT suspensions (40 mg/kg) given by gavage once a day, respectively. Tumor volume and body weight were measured and recorded every other day during the experiment process. All mice were sacrificed by spine and dissected 12 h after the last administration. Tumors, livers and spleens were excised and weighed. Tumor volume was calculated by equetion (4):

$$V = (a \cdot b^2)/2 \qquad (4)$$

Table 1. The IC50 values of the ICT-NRs, HICT-NRs, free ICT and free HICT against different tumor cell lines and HUVECs after incubation for 48 h.

Cells	IC50 (µg/mL)			
	HICT-NRs	Free HICT	ICT-NRs	Free ICT
MCF-7	$2.24 \pm 0.54^*$	8.04 ± 2.89	3.36 ± 1.24	4.04 ± 1.12
4T1	8.61 ± 2.59## ***	58.10 ± 8.06	26.63 ± 4.75\$\$	>50
PLC/PRF/5	$3.03 \pm 0.96^*$	8.41 ± 3.81	4.27 ± 1.89	5.05 ± 2.66
HepG2	$5.61 \pm 1.56^{***}$	>50	7.58 ± 3.37\$	13.27 ± 3.91
HUVECs	41.84 ± 8.97	59.26 ± 11.62	50.25 ± 7.32	53.04 ± 8.63

The results are presented as the mean $\pm$ SD, $n = 6$. $^{\$}p < 0.05$, $^{\$\$}p < 0.01$ vs. free ICT; $^*p < 0.05$, $^{***}p < 0.001$ vs. free HICT; $^{\#\#}p < 0.01$ vs. ICT nanorods.

where V is the tumor volume, a is the major axis length, and b is the minor axis length.

The tumor inhibition rate (TIR) was calculated by equation (5):

$$TIR\ (\%) = (1 - W_e/W_n) \times 100 \qquad (5)$$

where W_e is the mean tumor weight of experimental group and W_n is the mean tumor weight of NS group.

Statistical analysis

Statistical analysis of experimental data was calculated by independent-samples T-test and F-test using IBM SPSS Statistics software, Version 21 (IBM Corporation, USA). $p < 0.05$ was considered as statistically significant.

Results and discussions

Preparation of HICT-NRs and ICT-NRs

A simple antisolvent precipitation method was employed to prepare ICT or HICT nanosuspensions so as to solve their poor solubility and facilitate *in vivo* drug delivery. Both ICT and HICT were more easily soluble in DMSO than in ethanol, methanol and acetone, so DMSO was selected as the organic phase to dissolve ICT or HICT. Selection of a suitable stabilizer is quite important for the preparation and stability of the nanosuspensions, Pluronic F-127, F-68, mPEG2000-DSPE, TPGS, and mPEG2000-PCL2000 were tried as a stabilizer respectively, to prepare ICT or HICT nanorods at 25 °C and the starting drug/stabilizer feeding ratio was set as 1:1 (w/w). It turned out that all of the above stabilizers worked and led to the formation of ICT or HICT nanosuspensions, among which TPGS showed the best stabilizing effect, resulting in the smallest size, the narrowest size distribution and good zeta potential for both ICT and HICT nanorods (Supplementary Table S1). Therefore, TPGS was chosen as the optimal stabilizer to prepare ICT-NRs and HICT-NRs in the succeeding research. The high zeta potential of the resultant nanorods suggested good storage stability (Muller et al., 2001).

Furthermore, the higher HICT/TPGS feeding ratios (2:1,3:1 and 6:1) were also tried to prepare HICT-NRs, and the particle size of the resultant nanorods in different physiological media was investigated. Supplementary Table S2 showed that the increasing drug/stabilizer ratios resulted in a slightly larger particle size. This is a common seen phenomenon (Pagar & Vavia, 2014; Hong et al., 2016), as higher drug/

stabilizer ratio meant less stabilizer molecules to inhibit the growth of HICT crystals during the formation of nanosuspensions. The particle size stability data displayed, only when the drug-stabilizer ratio was 1:1, the prepared HICT nanorods were stable in all tested physiological media. The higher feeding ratios (2:1, 3:1, 6:1) all led to significant particle size enlargement or aggregation after 2 h of incubation in NS and PBS and consequently not suitable for further *in vivo* efficacy study. In consideration of size, drug loading content and stability, HICT/TPGS ratio of 1:1 was selected to prepare HICT-NRs for further investigation.

In some cases, temperature of antisolvent precipitation influences the particle size and stability of the obtained nanorods (Yang et al., 2015), so different temperatures (15 °C, 25 °C, 35 °C and 45 °C) were tested to prepare HICT-NRs at the same HICT/TPGS feeding ratio of 1:1. It turned out that 25 °C was the most proper temperature and the obtained HICT-NRs had the smallest particle size (202 nm), the narrowest size distribution (PDI value, 0.17) and the highest zeta potential (-22.9 mV) (Supplementary Table S3). In consequence, 25 °C was selected as the processing temperature for subsequent preparation of HICT-NRs.

HICT/TPGS feeding ratio of 1:1 and 25 °C also led to small particle size (Supplementary Table S1) and good stability in physiological media of HICT-NRs. Since the aim of this study was to compare the *in vivo* performance of ICT and HICT in the tumor treatment, no more optimization was performed for the preparation of ICT-NRs.

Characterizations of HICT-NRs and ICT-NRs

The mean particle size of the obtained ICT-NRs and HICT-NRs was 155.5 ± 1.5 nm and 201.7 ± 1.3 nm respectively (Figure 1(c) and Supplementary Table S1) with the PDI value being 0.16 ± 0.02 and 0.17 ± 0.07. The small PDI value indicated that both nanorods were nearly monodisperse. In addition, zeta potential of ICT-NRs and HICT-NRs was -19.5 ± 0.5 mV and -22.9 ± 0.6 mV; the DLC was respectively $43.30 \pm 0.22\%$ and $41.08 \pm 0.19\%$, respectively. 4 mg of ICT or HICT formed a turbid yellow suspension with a large amount of sediment when dispersed in 1 mL water (Supplementary Figure S1), while, in sharp contrast, ICT or HICT nanorods containing 4 mg/mL drug were homogenously yellow with light blue opalescence (Figure 1(d)) and can maintain stable more than 1 month at room temperature. The solubility of ICT and HICT in water determined by HPLC were both less than 1 µg/mL, nanorods could easily enhance the apparent solubility of ICT and HICT to more than 4000 times.

Transmission electron microscopy image (Figure 1(e,f)) revealed that both ICT-NRs and HICT-NRs were rod-like in shape, which was consistent with our previous study (Wang et al., 2020). Nanorods were rarely seen in flavonoid nanoparticles. It was reported nanorods had longer blood circulation time, more cellular uptake and tumor accumulation compared to disk and spherical nanoparticles (Banerjee et al., 2016; Yang et al., 2016).

The DSC investigation results were shown in Figure 2(a,b). ICT powder and its physical mixture with TPGS had an

Table 2. *In vivo* antitumor effects of different groups against MCF-7 bearing nude mice model.

Formulation	Tumor weight (g)	Inhibition rate (%)	Liver coefficient	Spleen coefficient
HICT-NRs *i.v.*	0.36 ± 0.16**#	72.18#	0.047 ± 0.003	0.002 ± 0.001
HICT-NRs *i.g.*	0.70 ± 0.20	46.87	0.045 ± 0.005	0.005 ± 0.001
Free HICT *i.g.*	0.81 ± 0.16	38.27	0.048 ± 0.002	0.004 ± 0.002
ICT-NRs *i.v.*	0.51 ± 0.12*◎*	60.70◎*	0.050 ± 0.003	0.003 ± 0.002
ICT-NRs *i.g.*	0.78 ± 0.08	40.64	0.042 ± 0.007	0.002 ± 0.001
Free ICT *i.g.*	0.84 ± 0.12	36.03	0.052 ± 0.004	0.003 ± 0.001
PTX injection *i.v.*	0.47 ± 0.04*	64.47	0.042 ± 0.002	0.002 ± 0.002
Normal saline	1.32 ± 0.24	NA	0.052 ± 0.006	0.003 ± 0.002

The results are presented as the mean ± SD, $n = 7$. $*p < 0.01$, $**p < 0.001$vs. normal saline; $\&p < 0.05$ vs. HICT-NRs i.g. group; $\#p < 0.05$ vs. free HICT i.g. group; $◎p < 0.05$ vs. ICT-NRs i.g. group; $*p < 0.05$ vs. free ICT i.g. group. The dosage is 40 mg/kg of all experiment group and 8 mg/kg of PTX injection group.

Table 3. *In vivo* antitumor effects of different groups against PLC/PRF/5- bearing nude mice model.

Formulation	Tumor weight(g)	Inhibition rate (%)	Liver coefficient	Spleen coefficient
HICT-NRs *i.v.*	0.12 ± 0.07*	63.1$^{\$}$##	0.042 ± 0.002	0.003 ± 0.002
HICT-NRs *i.g.*	0.24 ± 0.12	25.3$^{\$}$	0.047 ± 0.003	0.004 ± 0.001
Free HICT *i.g.*	0.28 ± 0.17	11.8$^{\$}$	0.044 ± 0.003	0.003 ± 0.001
ICT-NRs *i.v.*	0.15 ± 0.15*	52.5$^{\$}$◎**	0.042 ± 0.002	0.003 ± 0.002
ICT-NRs *i.g.*	0.25 ± 0.20	21.8$^{\$}$	0.048 ± 0.005	0.002 ± 0.001
Free ICT *i.g.*	0.29 ± 0.14	9.3$^{\$}$	0.042 ± 0.007	0.003 ± 0.001
PTX injection *i.v.*	0.06 ± 0.03**	80.6$^{\$}$	0.052 ± 0.004	0.003 ± 0.002
Normal saline	0.32 ± 0.23	NA	0.045 ± 0.007	0.002 ± 0.001

The results are presented as the mean ± SD, $n = 7$. $*p < 0.01$, $**p < 0.001$vs. normal saline; $\$p < 0.01$vs. PTX injection group; $\&p < 0.05$ vs. HICT-NRs i.g. group; $\#\#p < 0.01$ vs. free HICT i.g. group; $◎p < 0.05$ vs. ICT-NRs i.g. group; $**p < 0.01$ vs. free ICT i.g. group. The dosage is 40 mg/kg of all experiment group and 8 mg/kg of PTX injection group.

endothermic peak at about 250 °C indicating the existence of ICT crystalline. HICT powder and its physical mixture with TPGS both showed an acute endothermic peak at approximately 240 °C, which is corresponding HICT's melting point. However, ICT-NRs had two weak melting endothermic peaks separately at 160 °C and 250 °C, which meant ICT crystalline changed and most ICT exited in ICT-NRs as amorphous state. Similarly, HICT-NRs showed two melting endothermic peaks at 164.7 °C and 210.5 °C, indicating that crystalline form of HICT may be changed in the preparation process. XRD patterns of HICT and ICT powder, HICT-NRs and ICT-NRs, stabilizer (TPGS), and the physical mixture of HICT/ICT powder and TPGS were measured under consistent condition. Figure 2(c,d) demonstrated that ICT powder had a sharp diffraction peak of crystallinity at 5°, HICT powder had a sharp diffraction peak of crystallinity at 12°, suggesting crystalline structure existence in ICT and HICT powder. The diffraction pattern of the lyophilized ICT-NRs and HICT-NRs were both much weaker than that of bulk powder and the physical mixture. The results could prove that the crystalline form of ICT and HICT in nanorods had at least changed partially during the preparation of HICT-NRs.

The stability and hemolysis of HICT-NRs and ICT-NRs

Both ICT-NRs and HICT-NRs were comparatively stable in physiological medium including NS, isotonic glucose, PBS, artificial gastric and intestinal fluid after incubation at 37 °C for 8 h (Figure 3(a,b)). No aggregation and no significant particle size increase were observed.

To determine whether ICT or HICT nanorods could be stable in plasma, ICT or HICT nanorods were incubated with rat plasma for size change supervision. There are a variety of enzymes and serum albumins in plasma which can be

adsorbed to the surface of nanoparticles and transform surface properties, which would lead to size increasement or precipitation of nanoparticles(Hong et al., 2016). Figure 3(a,b) showed that the particle size of ICT-NRs (165 nm to 305 nm) and HICT-NRs (256 nm to 500 nm) both had size increasement after 8 h incubation, but there was no aggregation and ICT or HICT nanorods were still in uniform dispersion, so ICT or HICT nanorods could be still be regarded suitable for intravenous injection.

In the hemolysis test, different concentrations of ICT or HICT nanorods were mixed with rat erythrocytes, as shown in Supplementary Figure S2, 1 mg/mL and 2 mg/mL of ICT or HICT nanorods displayed no hemolysis at all; when the concentration increased to 4 mg/mL, the hemolysis rate was 1.3% for ICT-NRs and 1% for HICT-NRs; only 6% and 9% of hemolysis was observed for ICT-NRs and HICT-NRs respectively at 6 mg/mL. Since less than 5% of hemolysis was regarded as safe for intravenous administration, the above data demonstrated ICT or HICT nanorods were safe for intravenous administration at low dose.

The results of stability and hemolysis test suggested that ICT-NRs and HICT-NRs were suitable for intravenous administration as well as oral medication.

Drug release behavior of HICT-NRs and ICT-NRs

The cumulative dissolution profiles of ICT-NRs and HICT-NRs was quite similar as shown in Figure 3(c). There was an initial burst release at the first 2 h and the cumulative release reached 10.43% for ICT-NRs and 9.15% for HICT-NRs, which might be attributed to a quick diffusion of drug molecules attached on the surface of nanorods into the release media. Then ICT-NRs and HICT-NRs both displayed stable and gradual drug release. The cumulative release reached 80.53% for
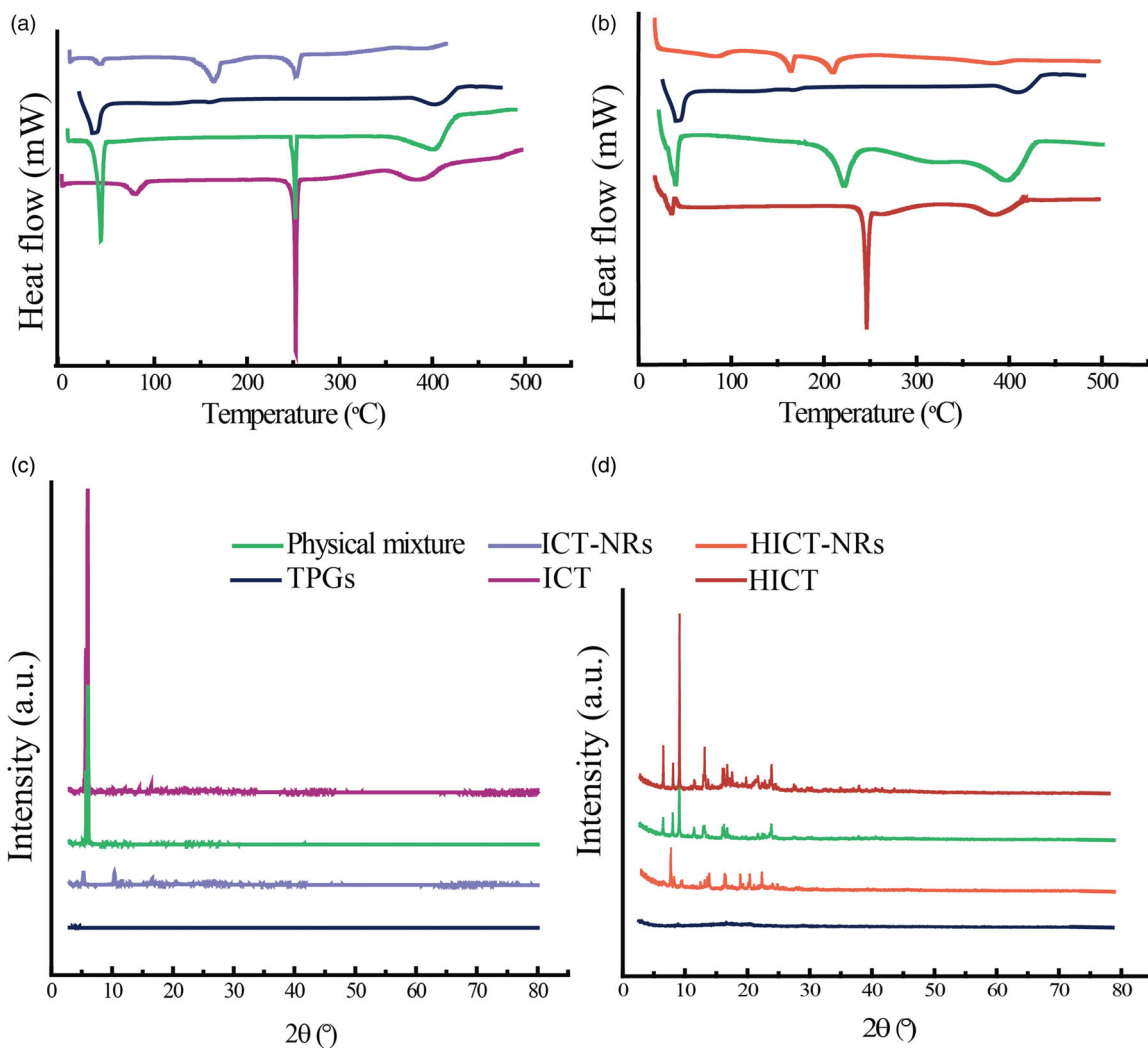
Figure 2. DSC thermograms XRD patterns. (a) DSC thermograms of the ICT bulk powder, stabilizer (TPGS), ICT-NRs, and the physical mixture of ICT bulk powder and TPGS. (b) DSC thermograms of the HICT bulk powder, stabilizer (TPGS), HICT-NRs, and the physical mixture of HICT bulk powder and TPGS. (c) XRD patterns of the ICT bulk powder, stabilizer (TPGS), ICT-NRs, and the physical mixture of ICT bulk powder and TPGS. (d) XRD patterns of the HICT bulk powder, stabilizer (TPGS), HICT-NRs, and the physical mixture of HICT bulk powder and TPGS.

ICT-NRs and 77.48% for HICT-NRs at 144 h. The release rate of ICT-NRs was slightly faster than that of HICT-NRs probably due to slightly smaller particle size. The release of ICT or HICT nanorods followed first-order release pattern.

ICT and HICT coarse suspensions (ICT or HICT bulk powder dispersed in deionized water) were examined as control groups, but nearly no drug was detected in the release media, and this may be due to their very poor solubility. The much higher cumulative release rate of ICT or HICT nanorods compared with the coarse suspensions of ICT and HICT could be ascribed to the small size of particles, much larger superficial area and the increased solubility of ICT or HICT nanorods as reported (Hong et al., 2016). The presence of TPGS molecules, whatever attached to the nanosuspensions or departed in the system, may also promote the drug release of ICT or HICT nanorods. In addition, the metastable state of ICT and HICT in nanorods also accelerated ICT and HICT release(Han et al., 2013). Meanwhile, the sustained and prolonged drug release will help avoid or reduce drug leakage during systemic circulation and ensure sufficient drug molecules arrive at tumor tissues.

In vitro *cytotoxicity assay*

Cytotoxicity of ICT-NRs and HICT-NRs against 4T1, MCF-7, PLC/PRF/5, HepG2 and HUVEC cells was assessed using MTT assay. As listed in Figure 4, both ICT-NRs and HICT-NRs inhibited the proliferation of the above 4 kinds of tumor cell lines in a dose-dependent manner, so did free drugs. But ICT-NRs and HICT-NRs exhibited higher cytotoxicity than the corresponding free drug against all examined cancer cell lines at nearly all tested drug concentrations. The calculated IC50 values (seen in Table 1) displayed that nanorods enhanced the cytotoxicity of ICT against different tumor cells especially 4T1 cells; and HICT-NRs notably enhanced *in vitro* aititumor activity by 2.5-21 times ($p < 0.05$, $p < 0.01$, or $p < 0.001$) against above tumor cell lines in contrast to free HICT. This may be explained by that ICT-NRs and HICT-NRs can be uptaken into tumor cells through nonspecific adsorption and endocytosis internalization (Fernández-Urrusuno et al., 1996; Dong et al., 2016), while free drugs can merely transported inside cells via passive diffusion. However, no significant
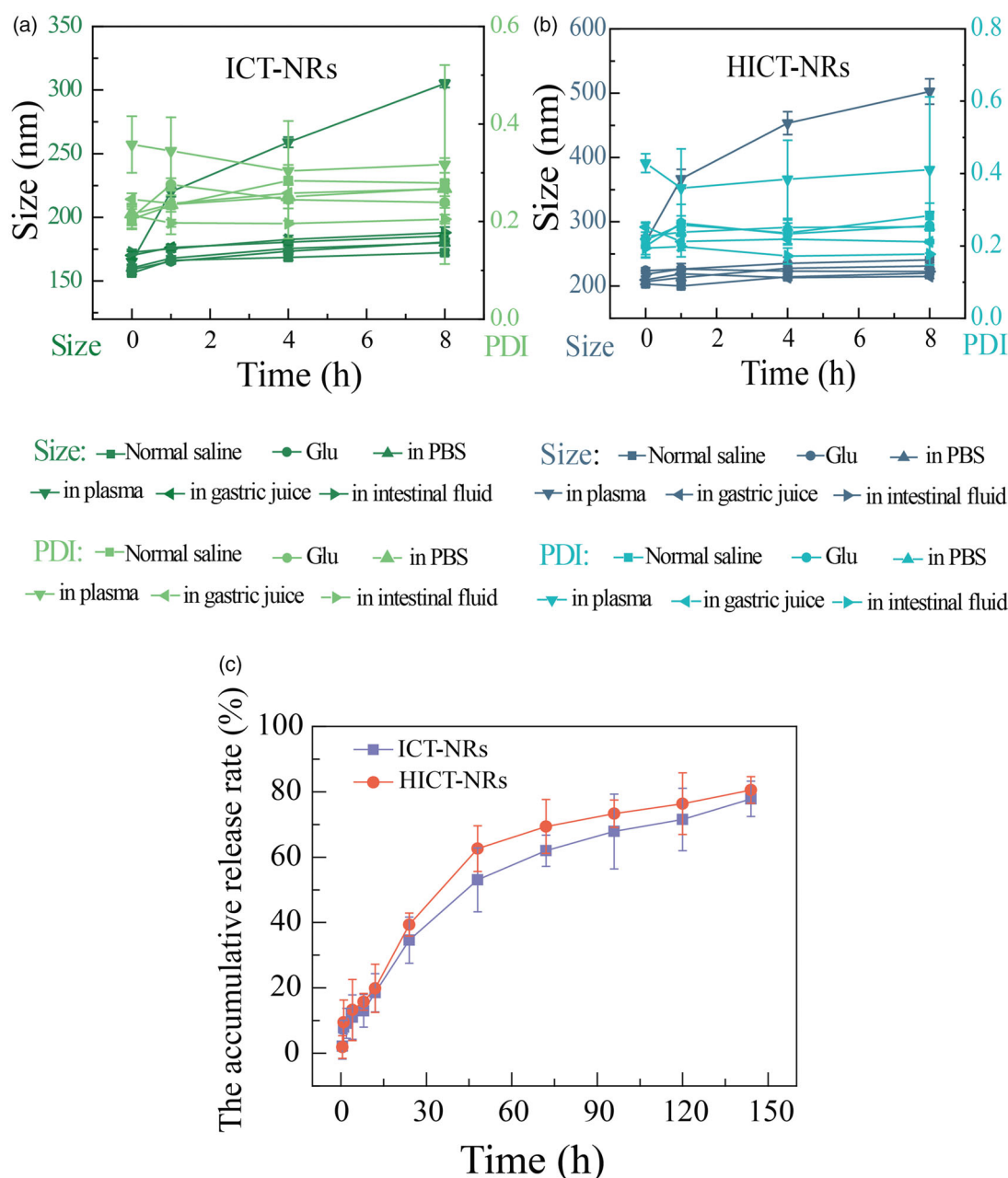
Figure 3. The stability and *in vitro* drug release profiles of ICT-NRs and HICT-NRs. (a) Particle size and PDI changes of the ICT-NRs after incubation in various physiological solutions at 37 °C until 8 h. (b) Particle size and PDI changes of the HICT-NRs after incubation in various physiological solutions at 37 °C until 8 h. (c) The *in vitro* drug release profiles of ICT-NRs and HICT-NRs in pH 7.4 PBS containing 0.5% (w/v) Tween80 at 37 °C (mean ± SD, $n = 3$).

increased toxicity was observed toward normal epithelial HUVEC cells (seen in Table 1, Supplementary Figure S3(a,b)).

What's more, HICT-NRs demonstrated slightly stronger cytotoxicity than ICT-NRs against the 4 tested tumor cell lines, although ICT-NRs had smaller particle size, suggesting of probable superior *in vivo* therapeutic efficacy over ICT-NRs. In addition, among all the examined cancer cell lines, MCF-7 cell line was most sensitive to ICT-NRs and HICT-NRs (IC50, 3.36 μg/mL and 2.24 μg/mL), followed by PLC/PRF/5 cell line (4.27 μg/mL and 3.03 μg/mL). So MCF-7 and PLC/PRF/5 bearing tumor mice models were used in the next *in vivo* study.

Cytotoxicity of TPGS and DMSO was also investigated as blank control (Supplementary Figure S3(c,d)). It was shown

that all the tested cell lines retained over 95% viability in 100 μg/mL of TPGS (the highest concentration of ICT or HICT nanorods in the MTT assay) after 48 h of incubation. This proved that TPGS is a safe stabilizer. In case of DMSO, almost 100% of the tested cell lines were still viable in the culture medium containing 0.1% DMSO (the highest DMSO concentration for free ICT or HICT solution in MTT assay), indicating no influence of DMSO on the cell growth in our study.

In vivo *antitumor activity*

The antitumor efficacy of the ICT or HICT nanorods were investigated using MCF-7 and PLC/PRF/5 tumor-bearing mice models. PTX injection was chosen as positive control. In our
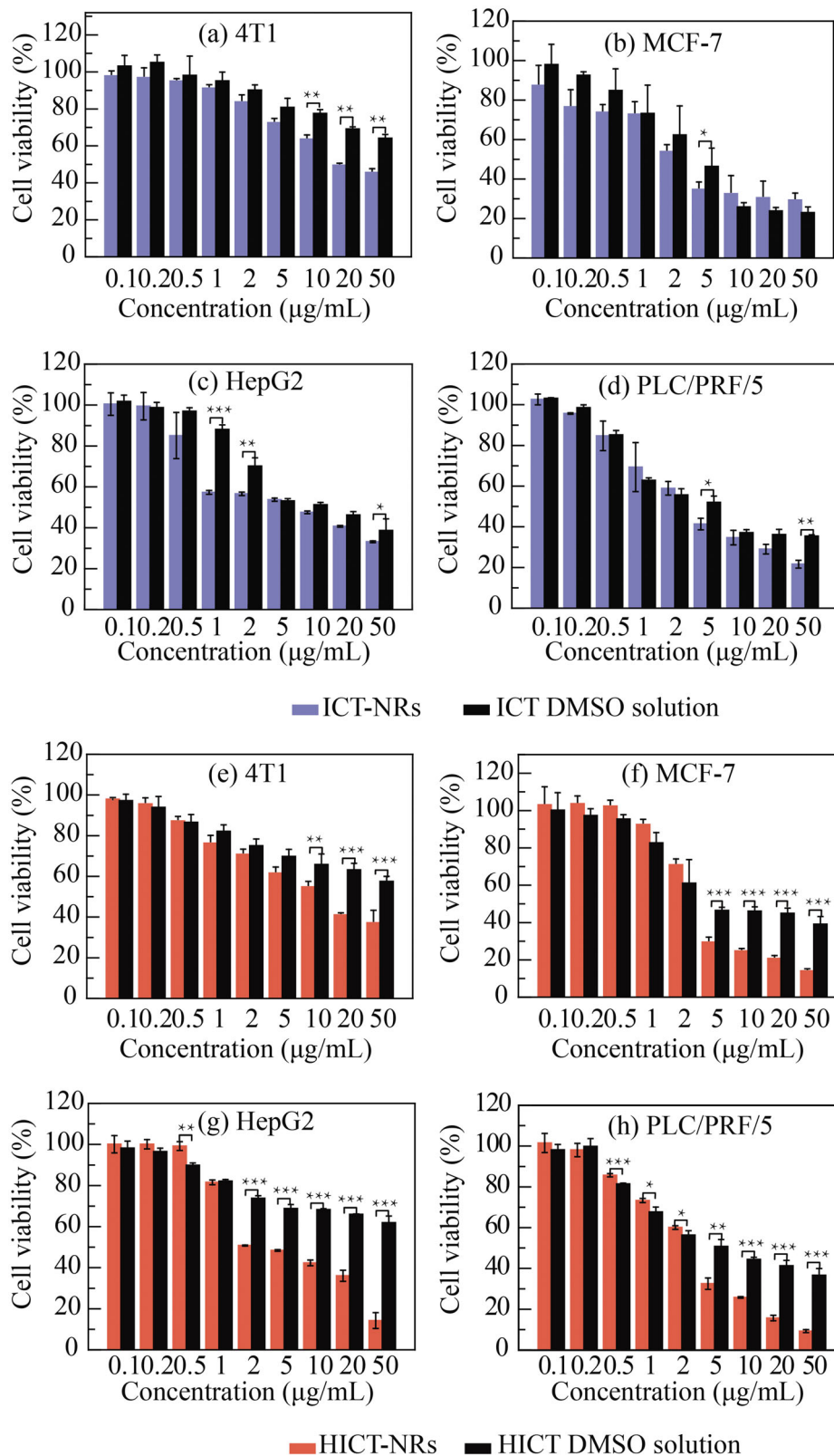
Figure 4. *In vitro* cytotoxicity of ICT/HICT-NRs and ICT/HICT DMSO solution on different cancer cell lines after 48 h of incubation (mean ± SD, $n = 6$) (mean ± SD, $n = 6$, $^*p < 0.05$, $^{**}p < 0.01$, and $^{***}p < 0.001$).

another experiment (Supplementary Figure S4), HICT-NRs displayed a dose-dependent manner in MCF-7 tumor-bearing mice. 40 mg/kg demonstrated the best tumor inhibition effect, so 40 mg/kg was selected as the experimental dose to

compare the *in vivo* antitumor efficacy between ICT and HICT.

For MCF-7 tumor-bearing mice model, the tumor volume growth curves are pictured in Figure 5(a). NS group showed
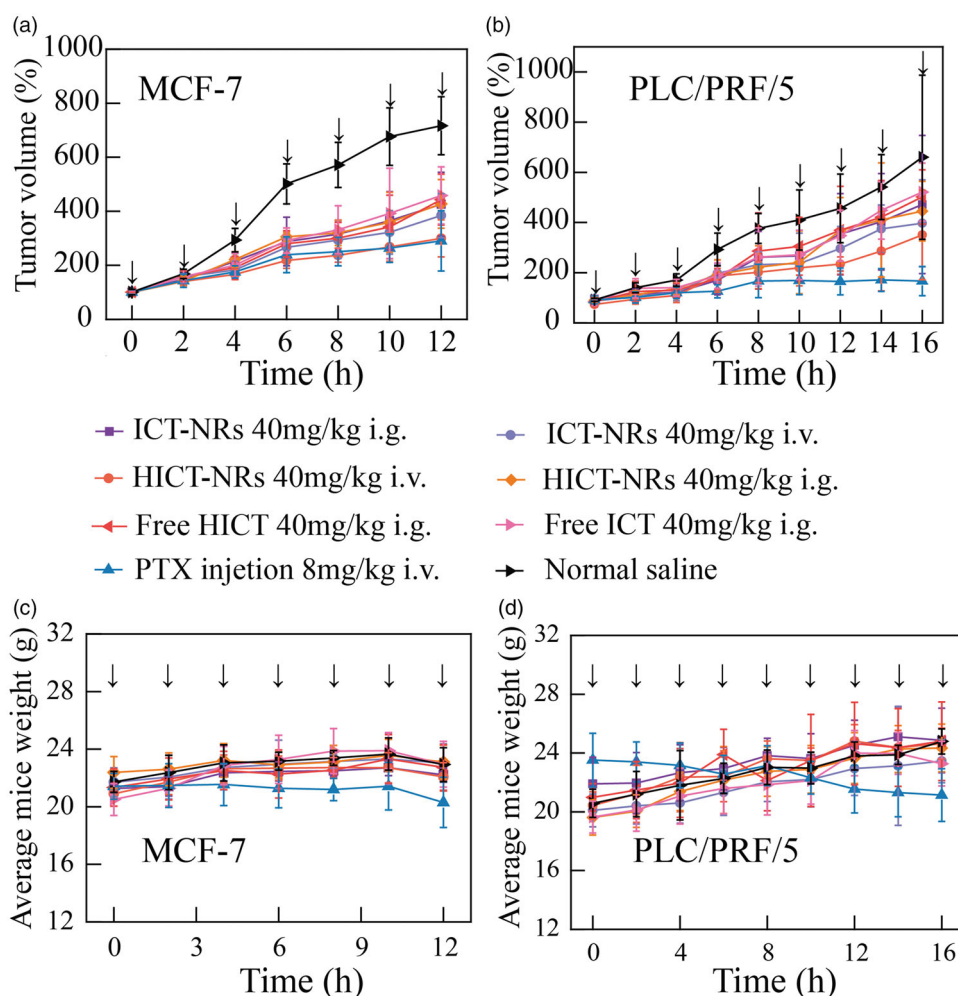
Figure 5. *In vivo* antitumor activity of ICT/HICT-NRs against MCF-7 and PLC/PRF/5 tumor-bearing mice. (a) The growth of tumor volume over time of each group against MCF-7 tumor-bearing mice. (b) The growth of tumor volume over time of each group against PLC/PRF/5 tumor-bearing mice. (c) Average body weight change of mice over time of each group against MCF-7 tumor-bearing mice. (d) Average body weight change of mice over time of each group against PLC/PRF/5 tumor-bearing mice (mean ± SD, $n = 7$, ↓ represents administration times).

fastest tumor growth, while all other groups showed much slower tumor growth, among which the intravenously injected nanorods resulted in the least tumor volume. The tumor inhibition rate (TIR) data (Table 2) showed that the orally administrated ICT-NRs and HICT-NRs had better antitumor efficacy than free ICT and HICT suspensions (40.64% vs. 36.03% for ICT; 46.87% vs. 38.27% for HICT), suggesting that nanorods had higher bioavailability than coarse suspensions. Nanoscale particles can promote ICT or HICT accumulation in tumor through enhanced permeability and retention (EPR) effect (Prabhakar et al., 2013). As expected, intravenous administrated nanorods greatly enhanced the anti-tumor efficacy than oral administration (TIR, 60.71% vs. 40.64% for ICT-NRs, $p < 0.05$; 78.12% vs. 46.87% for HICT-NRs, $p < 0.05$), due to 100% bioavailability and the presence of the EPR effect. Obviously, HICT-NRs were more effective than ICT-NRs whatever orally or intravenously administrated (TIR, 72.18% vs. 60.71%, *i.v.*; 46.87% vs. 40.64%, *i.g.*), even better than the positive control (PTX injection, 8 mg/kg) (72.18% vs. 64.47%, Table 2), indicating good *in vivo* anti-tumor efficacy and promising prospect for new drug development.

For PLC/PRF/5 tumor-bearing mice model, the tumor volume change curves were shown in Figure 5(b). NS group

showed fastest tumor volume growth, but the tumor growth of other groups failed to be as slow as in MCF-7 tumor-bearing mice model except for PTX injections. Similarly. intravenously injected ICT-NRs and HICT-NRs had a slow tumor growth compared to the oral administrated nanorods and free ICT or HICT groups.

The TIR data of different groups against PLC/PRF/5 tumor were shown in Table 3. PTX injection demonstrated an excellent tumor inhibition effect with an inhibition rate of 80.6%. Unexpectedly, the inhibition rate was only 9.3% and 11.8% respectively for free ICT group and free HICT group, 21.8% and 25.3% for orally taken ICT-NRs and HICT-NRs, indicating low therapeutic efficacy of oral administration. Intravenously injected ICT-NRs and HICT-NRs achieved much higher TIR (52.5% and 63.1% respectively) than oral administration ($p < 0.05$), but far from the 80.2% TIR of PTX injections ($p < 0.01$). Similarly, HICT-NRs still showed a little stronger antitumor efficacy than ICT-NRs in this tumor model (TIR, 63.1% vs. 52.5%).

The body weight change profiles for MCF-7 and PLC/PRF/5 tumor-bearing mice models are depicted in Figure 5(c,d), the liver and spleen indexes are shown in Tables 2 and 3, all being important indicators to understand the systematic

toxicity of the tested drugs. In both mice model, all the experimental groups showed insignificant difference in liver and spleen indexes in comparison with NS group, and no obvious body weight reduction was observed except for PTX injection group. This indicated that PTX injection was a little toxic to mice, in contrast, ICT or HICT nanorods possessed good biosafety and low systematic toxicity.

It was apparent that both ICT-NRs and HICT-NRs exhibited better inhibition rate toward MCF-7 tumor than PLC/PRF/5 tumor (TIR, ICT-NRs: 60.7% vs. 52.5%; HICT-NRs: 72.1% vs. 63.1%), indicating breast cancer may be priority clinic indication for HICT and ICT when developed for a new drug. Whatever in MCF-7 or in PLC/PRF/5 tumor bearing mice model, HICT-NRs was superior to ICT-NRs in the therapeutic efficacy. Since ICT has been in phase III clinic trial for the treatment of hepatic tumor, it is reasonable to believe HICT will probably be a more promising antitumor agent than ICT to be used in clinic in the future.

For this purpose, the acute toxicity trial was performed for HICT-NRs. It turned out that even at the highest dose of 250 mg/kg that could be achieved, intravenous administration of HICT-NRs resulted in no death among tested 10 Kunming mice. The result meant LD50 of HICT-NRs was much more than 250 mg/kg, suggesting that HICT-NRs could be very promising to be a new antitumor drug with good effectives and safety.

Conclusion

ICT has been studied as an effective antitumor agent for many years and now in phase III clinic trial, but little attention had been paid to HICT, another flavonoid compound isolated from the same plant with quite similar chemical structure to ICT. In this study, HICT-NRs and ICT-NRs were successfully prepared using TPGS as a stabilizer and their *in vitro* and *in vivo* antitumor activity were compared for the first time. The obtained ICT-NRs and HICT-NRs had close diameter of 155.5 nm and 201.7 nm. Both ICT-NRs and HICT-NRs had high drug loading content ($43.30 \pm 0.22\%$ vs. $41.08 \pm 0.19\%$), excellent stability in different physiological media and a sustaining drug release manner for 140 h. At the same dose of 40 mg/kg, HICT-NRs achieved significantly better *in vivo* therapeutic efficacy than ICT-NRs (TIR, 72.1% vs 60.7%) and even better than 8 mg/kg of PTX injections (TIR, 64.4%) in MCF-7 tumor-bearing mice model. As for PLC/PRE/5 tumor-bearing mice model, HICT-NRs also showed slightly better tumor inhibition than ICT-NRs (63.1% vs. 52.5%, both at 40 mg/kg). No death was observed at the highest *i.v.* dose of 240 mg/kg of HICT-NRs in the acute toxic trial on mice, suggesting good safety. These results demonstrated that HICT is very promising to be transformed into a new agent in the future for tumor treatment, as does ICT.

Author contributions

Conceptualization, XT.W.; methodology, HW.L and YJ.L; investigation, HW.L and H.A.; resources, XT.W and X.C.; data curation, H.A and JX.F.; writing – original draft preparation, HW.L.; writing – review and editing, YF.G and XY.Y.; visualization, H.A. and JX.F; supervision, JX.F.; project administration, MH.H. and X C; funding acquisition, XT.W and X. C. All authors have read and agreed to the published version of the manuscript.

Disclosure statement

The author reports no conflicts of interest in this work.

References

Banerjee A, Qi J, Gogoi R, et al. Role of nanoparticle size, shape and surface chemistry in oral drug delivery. J Control Release. 2016;238: 176–185.

Commission, C. P. (2010). Pharmacopeia of the People's Republic of China Version 2010. Beijing: Chemical Industry Press.

Dong F, Dong X, Zhou L, et al. (2016). Doxorubicin-loaded biodegradable self-assembly zein nanoparticle and its anti-cancer effect: Preparation, in vitro evaluation, and cellular uptake. Colloids Surf B Biointerfaces 140:324–31.

Fernández-Urrusuno R, Fattal E, Rodrigues JM, et al. (1996). Effect of polymeric nanoparticle administration on the clearance activity of the mononuclear phagocyte system in mice. J Biomed Mater Res 31: 401–8.

Guo Y, Zhang X, Meng J, Wang ZY. (2011). An anticancer agent icaritin induces sustained activation of the extracellular signal-regulated kinase (ERK) pathway and inhibits growth of breast cancer cells. Eur J Pharmacol 658:114–22.

Han H, Xu B, Hou P, et al. (2015). Icaritin Sensitizes Human Glioblastoma Cells to TRAIL-Induced Apoptosis. Cell Biochem Biophys 72:533–42.

Han M, Liu X, Guo Y, et al. (2013). Preparation, characterization, biodistribution and antitumor efficacy of hydroxycamptothecin nanosuspensions. Int J Pharm 455:85–92.

Han M, Yu X, Guo Y, et al. (2014). Honokiol nanosuspensions: preparation, increased oral bioavailability and dramatically enhanced biodistribution in the cardio-cerebro-vascular system. Colloids Surf B Biointerfaces 116:114–20.

Han S, Gou Y, Jin D, et al. (2018). Effects of Icaritin on the physiological activities of esophageal cancer stem cells. Biochem Biophys Res Commun 504:792–6.

Hao H, Zhang Q, Zhu H, et al. (2019). Icaritin promotes tumor T-cell infiltration and induces antitumor immunity in mice. Eur J Immunol 49: 2235–44.

He J, Wang Y, Duan F, et al. (2010). Icaritin induces apoptosis of HepG2 cells via the JNK1 signaling pathway independent of the estrogen receptor. Planta Med 76:1834–9.

Hong J, Li Y, Li Y, et al. (2016). Annonaceous acetogenins nanosuspensions stabilized by PCL-PEG block polymer: significantly improved antitumor efficacy. IJN Volume 11:3239–53.

Hong J, Li Y, Xiao Y, et al. (2016). Annonaceous acetogenins (ACGs) nanosuspensions based on a self-assembly stabilizer and the significantly improved anti-tumor efficacy. Colloids Surf B Biointerfaces 145: 319–27.

Hu J, Yang T, Xu H, et al. (2016). A novel anticancer agent icaritin inhibited proinflammatory cytokines in TRAMP mice. Int Urol Nephrol 48: 1649–55.

Huang X, Zhu D, Lou Y. (2007). A novel anticancer agent, icaritin, induced cell growth inhibition, G1 arrest and mitochondrial transmembrane potential drop in human prostate carcinoma PC-3 cells. Eur J Pharmacol 564:26–36.

Lai X, Ye Y, Sun C, et al. (2013). Icaritin exhibits anti-inflammatory effects in the mouse peritoneal macrophages and peritonitis model. Int Immunopharmacol 16:41–9.

Li C, Li Q, Mei Q, Lu T. (2015). Pharmacological effects and pharmacokinetic properties of icariin, the major bioactive component in Herba Epimedii. Life Sci 126:57–68.

Li C, Peng W, Song X, et al. (2016). Anticancer effect of icaritin inhibits cell growth of colon cancer through reactive oxygen species, Bcl-2 and cyclin D1/E signaling. Oncol Lett 12:3537–42.

Li Q, Huai L, Zhang C, et al. (2013). Icaritin induces AML cell apoptosis via the MAPK/ERK and PI3K/AKT signal pathways. Int J Hematol 97:617–23.

Li S, Priceman SJ, Xin H, et al. (2013). Icaritin inhibits JAK/STAT3 signaling and growth of renal cell carcinoma. PLoS One 8:e81657.

Li X, Hu Y, He L, et al. (2012). Icaritin inhibits T cell activation and prolongs skin allograft survival in mice. Int Immunopharmacol 13:1–7.

Li Z, Meng X, Jin L. (2016). Icaritin induces apoptotic and autophagic cell death in human glioblastoma cells. Am J Transl Res 8:4628–43.

Li ZJ, Yao C, Liu SF, et al. (2014). Cytotoxic effect of icaritin and its mechanisms in inducing apoptosis in human burkitt lymphoma cell line. Biomed Res Int 2014:391512

Liao J, Liu Y, Wu H, et al. (2016). The role of icaritin in regulating Foxp3/IL17a balance in systemic lupus erythematosus and its effects on the treatment of MRL/lpr mice. Clin Immunol 162:74–83.

Liu DF, Li YP, Ou TM, et al. (2009). Synthesis and antimultidrug resistance evaluation of icariin and its derivatives. Bioorg Med Chem Lett 19:4237–40.

Liu P, Jin X, Lv H, et al. (2014). Icaritin ameliorates carbon tetrachloride-induced acute liver injury mainly because of the antioxidative function through estrogen-like effects. In Vitro Cell Dev Biol Anim 50:899–908.

Lu PH, Chen MB, Liu YY, et al. (2017). Identification of sphingosine kinase 1 (SphK1) as a primary target of icaritin in hepatocellular carcinoma cells. Oncotarget 8:22800–10.

Muller RH, Jacobs C, Kayser O. (2001). Nanosuspensions as particulate drug formulations in therapy. Rationale for development and what we can expect for the future. Adv Drug Deliv Rev 47:3–19.

Pagar KP, Vavia PR. (2014). Naltrexone-loaded poly[La-(Glc-Leu)] polymeric microspheres for the treatment of alcohol dependence: in vitro characterization and in vivo biocompatibility assessment. Pharm Dev Technol 19:385–94.

Pan XW, Li L, Huang Y, et al. (2016). Icaritin acts synergistically with epirubicin to suppress bladder cancer growth through inhibition of autophagy. Oncol Rep 35:334–42.

Prabhakar U, Maeda H, Jain RK, et al. (2013). Challenges and key considerations of the enhanced permeability and retention effect for nanomedicine drug delivery in oncology. Cancer Res 73:2412–7.

Sun F, Indran IR, Zhang ZW, et al. (2015). A novel prostate cancer therapeutic strategy using icaritin-activated arylhydrocarbon-receptor to co-target androgen receptor and its splice variants. Carcinogenesis 36:757–68.

Sun F, Zhang ZW, Tan EM, et al. (2016). Icaritin suppresses development of neuroendocrine differentiation of prostate cancer through inhibition of IL-6/STAT3 and Aurora kinase A pathways in TRAMP mice. Carcinogenesis 37:701–11.

Sun L, Chen W, Qu L, et al. (2013). Icaritin reverses multidrug resistance of HepG2/ADR human hepatoma cells via downregulation of MDR1 and P-glycoprotein expression. Mol Med Rep 8:1883–7.

Tiong CT, Chen C, Zhang SJ, et al. (2012). A novel prenylflavone restricts breast cancer cell growth through AhR-mediated destabilization of ERα protein. Carcinogenesis 33:1089–97.

Tong JS, Zhang QH, Huang X, et al. (2011). Icaritin causes sustained ERK1/2 activation and induces apoptosis in human endometrial cancer cells. PLoS One 6:e16781.

Wang C, Wu P, Shi JF, et al. (2015). Synthesis and cancer cell growth inhibitory activity of icaritin derivatives. Eur J Med Chem 100:139–50.

Wang X, Zheng N, Dong J, et al. (2017). Estrogen receptor-α36 is involved in icaritin induced growth inhibition of triple-negative breast cancer cells. J Steroid Biochem Mol Biol 171:318–27.

Wang XF, Wang J. (2014). Icaritin suppresses the proliferation of human osteosarcoma cells in vitro by increasing apoptosis and decreasing MMP expression. Acta Pharmacol Sin 35:531–9.

Wang Y, Huang T, Li H, et al. (2020). Hydrous icaritin nanorods with excellent stability improves the in vitro and in vivo activity against breast cancer. Drug Deliv 27:228–37.

Wang Z, Wang H, Wu J, et al. (2009). Enhanced co-expression of beta-tubulin III and choline acetyltransferase in neurons from mouse embryonic stem cells promoted by icaritin in an estrogen receptor-independent manner. Chem Biol Interact 179:375–85.

Wang ZQ, Lou YJ. (2004). Proliferation-stimulating effects of icaritin and desmethylicaritin in MCF-7 cells. Eur J Pharmacol 504:147–53.

Wo YB, Zhu DY, Hu Y, et al. (2008). Reactive oxygen species involved in prenylflavonoids, icariin and icaritin, initiating cardiac differentiation of mouse embryonic stem cells. J Cell Biochem 103:1536–50.

Wu T, Wang S, Wu J, et al. (2015). Icaritin induces lytic cytotoxicity in extranodal NK/T-cell lymphoma. J Exp Clin Cancer Res 34:17–0133.

Yan C, Zhao YH, Jia XB, Hu M. (2008). Intestinal absorption mechanisms of prenylated flavonoids present in the heat-processed Epimedium koreanum Nakai (Yin Yanghuo). Pharm Res. 25:2190–9.

Yang H, Chen Z, Zhang L, et al. Mechanism for the cellular uptake of targeted gold nanorods of defined aspect ratios. Small 2016;12:5178–5189.

Yang L, Jiang J, Hong J, et al. (2015). High Drug Payload 10-Hydroxycamptothecin Nanosuspensions Stabilized by Cholesterol-PEG: In Vitro and In Vivo Investigation. J Biomed Nanotechnol 11:711–21.

Ye HY, Lou YJ. (2005). Estrogenic effects of two derivatives of icariin on human breast cancer MCF-7 cells. Phytomedicine 12:735–41.

Zhang C, Li H, Jiang W, et al. (2016). Icaritin inhibits the expression of alpha-fetoprotein in hepatitis B virus-infected hepatoma cell lines through post-transcriptional regulation. Oncotarget 7:83755–66.

Zhang SQ, Zhang SZ. (2017). Oral absorption, distribution, metabolism, and excretion of icaritin in rats by Q-TOF and UHPLC-MS/MS. Drug Test Anal 9:1604–10.

Zhang SQ. (2016). Dynamic Biodistribution of Icaritin and Its Phase-II Metabolite in Rat Tissues by Ultra-High Performance Liquid Chromatography-Tandem Mass Spectrometry. Anal Sci 32:631–7.

Zhang W, Xing B, Yang L, et al. (2015). Icaritin Attenuates Myocardial Ischemia and Reperfusion Injury Via Anti-Inflammatory and Anti-Oxidative Stress Effects in Rats. Am J Chin Med 43:1083–97.

Zhao H, Guo Y, Li S, et al. (2015). A novel anti-cancer agent Icaritin suppresses hepatocellular carcinoma initiation and malignant growth through the IL-6/Jak2/Stat3 pathway. Oncotarget 6:31927–43.

Zheng Q, Liu WW, Li B, et al. (2014). Anticancer effect of icaritin on human lung cancer cells through inducing S phase cell cycle arrest and apoptosis. J Huazhong Univ Sci Technol Med Sci 34:497–503.

Zheng ZG, Zhang X, Zhou YP, et al. (2017). Anhydroicaritin, a SREBPs inhibitor, inhibits RANKL-induced osteoclastic differentiation and improves diabetic osteoporosis in STZ-induced mice. Eur J Pharmacol 809:156–62.

Zhou C, Chen Z, Lu X, et al. (2016). Icaritin activates JNK-dependent mPTP necrosis pathway in colorectal cancer cells. Tumour Biol 37:3135–44.

Zhou C, Gu J, Zhang G, et al. (2017). AMPK-autophagy inhibition sensitizes icaritin-induced anti-colorectal cancer cell activity. Oncotarget 8:14736–47.

Zhu DY, Lou YJ. (2005). Inducible effects of icariin, icaritin, and desmethylicaritin on directional differentiation of embryonic stem cells into cardiomyocytes in vitro. Acta Pharmacol Sin 26:477–85.

Zhu J, Li Z, Zhang G, et al. (2011). Icaritin shows potent anti-leukemia activity on chronic myeloid leukemia in vitro and in vivo by regulating MAPK/ERK/JNK and JAK2/STAT3/AKT signalings. PLoS One 6:e23720.

Zhu S, Wang Z, Li Z, et al. (2015). Icaritin suppresses multiple myeloma, by inhibiting IL-6/JAK2/STAT3. Oncotarget 6:10460–72.